AD-A230 383

12-17-90

Office of Naval Research

Contract N00014-89-J-1276

Technical Report No. UWA/DME/TR-90/68

DYNAMIC FRACTURE ANALYSIS BY MOIRE INTERFEROMETRY

by

K. Arakawa, R.H. Drinnon, M. Kosai and A.S. Kobayashi

December 1990

DTIC
ELECTE
JAN 07 1991
S D
D

The research reported in this technical report was made possible through support extended to the Department of Mechanical Engineering, University of Washington, by the Office of Naval Research under Contract N00014-89-J-1276. Reproduction in whole or in part is permitted for any purpose of the United States Government.

DISTRIBUTION STATEMENT A
Approved for public release;
Distribution Unlimited

Department of Mechanical Engineering

College of Engineering

University of Washington

91 1 3 228

DYNAMIC FRACTURE ANALYSIS BY DYNAMIC MOIRE INTERFEROMETRY

K. Arakawa*, R.H. Drinnon, Jr.**, M. Kosai*** and A.S. Kobayashi****

ABSTRACT

Dynamic moire interferometry was used to measure separately the u- and v-displacement fields surrounding a rapidly propagating crack tip in Homalite-100 and 7075-T6 aluminum alloy plates. This transient crack tip displacement data was then used to compute the dynamic stress intensity factor and the remote stress component. J-integral values was also estimated using the static approximate procedure, ~~of Kang et al~~. This static analysis provided the correct J when the contour integral was taken within 3 mm of the crack tip

INTRODUCTION

For the past two decades, brittle polymers have been used as a model material for identifying the dynamic fracture parameter(s) which govern rapid crack propagation. The two most popular experimental techniques used for such studies were the whole field techniques of dynamic photoelasticity [1,2] and dynamic caustics [3,4,5]. A third whole field technique, i.e. dynamic moire technique, was never developed to the sophistication of photoelasticity and caustics despite its early use in the mid 60's [6,7]. More recently, static moire technique, with detailed error analysis, has been used to determine the stress intensity factor (SIF) [8]. Static moire interferometry and geometric moire techniques have also been used to study the path independency of the J-integral and the validity of the HRR field in elastic-plastic fracture mechanics [9,10].

This paper reports on an experimental procedure for extracting the dynamic SIF and remote stress component from the transient crack-tip displacement field of a rapidly propagating crack in Homalite-100 and 7075-T6 aluminum alloy, single-edged notched (SEN) specimens.

* Associate Professor, Research Institute For Applied Mechanics, Kyushu University 87, Kasuga 816, Japan.

** Boeing Commercial Airplane Group, P.O. Box 3707, Seattle, WA 98124

*** Graduate Student, Department of Mechanical Engineering, University of Washington, Seattle, WA 98195.

**** Professor, Department of Mechanical Engineering, University of Washington, Seattle, WA 98195.

THEORETICAL BACKGROUND

Dynamic Crack Tip Displacement Field

The asymptotic crack tip displacement field for a constant velocity crack is given as an infinite series in Reference [11]. When such a higher order series of the crack tip displacement equations is used in the data reduction procedure for SIF determination, a large number of displacement measurements from a large crack tip region is needed. In dynamic analysis, however, the data points from a large crack tip region will mask the possible small but sharp transient stress gradients within this region as demonstrated by an error analysis in Reference [12]. On the other hand, the inevitable caustics as well as the possible nonlinear zone surrounding the crack tip exclude the use of the very-near crack-tip data thus limiting the available crack tip region for data analysis to a narrow ring region surrounding the crack tip. In view of the above, only the $1/\sqrt{r}$ term in the crack tip stress field and the constant term, or the two displacement terms involving the dynamic stress intensity factor and the remote stress component, K_I^{dyn} and σ_{ox}^{dyn}, respectively were considered in this study. In terms of a polar coordinate, (r, θ), with the origin at the moving crack tip, the displacement parallel and perpendicular to the crack tip, u and v, can be represented as [11];

$$u = \frac{K_I^{dyn} B_I(c)}{\mu}\sqrt{\frac{2}{\pi}}\left\{r_1^{\frac{1}{2}}\cos\frac{\theta_1}{2} - \frac{2\beta_1\beta_2}{1+\beta_2^2}\, r_2^{\frac{1}{2}}\cos\frac{\theta_2}{2}\right\}$$

$$+\frac{1}{2\mu}\sigma_{ox}^{dyn}\cdot B_I(c)\left\{r_1\cos\theta_1 - \frac{1+\beta_2^2}{2} r_2\cos\theta_2\right\} \qquad (1)$$

$$v = \frac{K_I^{dyn} B_I(c)}{\mu}\sqrt{\frac{2}{\pi}}\left\{-\beta_1 r_1^{\frac{1}{2}}\sin\frac{\theta_1}{2} + \frac{2\beta_1}{1+\beta_2^2}\, r_2^{\frac{1}{2}}\sin\frac{\theta_2}{2}\right\}$$

$$+\frac{1}{2\mu}\sigma_{ox}^{dyn}\cdot B_I(c)\left\{-\beta_1 r_1\sin\theta_1 + \frac{1+\beta_2^2}{2\beta_2} r_2\cdot\sin\theta_2\right\} \qquad (2)$$

where

Accesion For
NTIS CRA&I
DTIC TAB
Unannounced
Justification
By
Distribution /
Availability
Dist
A-1

QUALITY INSPECTED 4

$$\beta_1^2 = 1 - \frac{C^2}{C_1^2} \qquad \beta_2^2 = 1 - \frac{C^2}{C_2^2}$$

$$r_j e^{i\theta j} = x + i\beta_j y$$

$$B_I(c) = \frac{1+\beta_2^2}{4\beta_1\beta_2 - (1+\beta_2^2)^2} \tag{3}$$

x and y are the orthogonal coordinates with its origin at the moving crack tip, C_1 and C_2 are the dilatational and distortional wave velocities, respectively, C is the crack velocity. and μ is the shear modulus.

Note that for the asymptotic equations of Equations (1) and (2) to be valid, $r < d/10$ where d is the governing characteristic length which is normally the crack length or the remaining ligament, whichever is smaller, of a fracture specimen.

Dynamic Crack Curving and Branching

The physical significance of the remote stress component, σ_{ox}^{dyn}, in linear elasto-dynamic fracture mechanics is its influence on crack curving and crack branching. The mechanics of elastic crack curving as well as crack branching was studied by one of the authors and his colleague [13,14]. The dynamic crack curving criterion postulates that the state of stress ahead of a crack tip dictates the direction of crack propagation. The crack curving criterion thus assumes that when the circumferential stress within a prescribed crack tip region attains a maximum value off the axis of a self-similar crack extension, crack curving will occur. This maximum condition, which is based on linear elasto-dynamic fracture mechanics (LEFM), results in a characteristic crack tip distance, r_o, in which the propagating crack will deviate from its axis. For a crack propagating at a constant velocity, this value is

$$r_o = \frac{9}{128\pi}\left[\frac{K_1}{\sigma_{ox}} V_o(C,C_1,C_2)\right]^2 \tag{4}$$

where

$$V_o(C,C_1,C_2) = B_1(C)\left\{-(1+\beta_2^2)(2-3\beta_1^2) - \frac{4\beta_1\beta_2}{1+\beta_2^2}(14+3\beta_2^2) - 16\beta_1(\beta_1-\beta_2) + 16(1+\beta_1^2)\right\} \tag{5}$$

The elastic crack curving criterion requires that $r_o < r_c$ for the crack to curve away from its axis where r_c is a material constant which specifies the characteristic crack tip region in which the off-axis micro-cracks enlarge and connect to the main crack tip. The angular deviation of the crack from its original direction of self-similar crack extension is given in [13].

In the presence of a large driving force, i.e. a large K_I^{dyn}, the crack will bifurcate in order to shed the excess driving force and thus results in crack branching where the crack branching angle is governed by the crack curving criterion. This crack branching criterion was used successfully to correlate the predicted and measured crack branching angle and the estimated crack branching stress intensity factor, K_{IB}, [14].

J-estimation Procedure

While the COD approach based on Equations (1) and (2) is the preferred procedure for obtaining K_I^{dyn}, often the COD in the vicinity of the crack tip is obscured by the caustics and its trailing plastic zone. On the other hand, the J-integral approach, which circumvents this effect of small-scale yielding, requires simultaneous measurements of the u and v fields [9,10] as well as the particle velocity and acceleration within the contour of integration [11]. These requirements are extremely difficult to satisfy experimentally and thus the feasibility of using the "static J-estimation" procedure was explored in this paper.

The static J-estimation procedure consists of approximating the two dimensional states of stress and strain with uniaxial states of stress and strain. For a SEN specimen shown in Figure 1, this replacement provides the exact J if the contour integration is taken along the specimen boundaries and the crack faces. If the two horizontal paths in Figure 1 are sufficiently remote from the crack tip and if the SEN specimen is subjected to a simple loading, then this replacement also provides the exact states. Thus the J evaluated along the most remote contour in Figure 1 using the static J-estimation procedure will yield the correct static J-integral. Some of the mathematical expressions associated with the J-estimation procedure are listed in the following.

For plane problems governed by nonlinear elasticity and deformation plasticity, the static J-integral along the traction-free vertical edges of segments 12 and 34 in Figure 1 is:

$$J_V = \int_{12+34} W\, dy = (\Sigma W_i\, \Delta y_i)_{12} + (\Sigma W_i\, \Delta y_i)_{34} \tag{5}$$

where i is the ith segment of the contour and W is the strain energy density.

If horizontal segment 23 is sufficiently far away from the crack, we can assume that the shear stress, τ_{xy}, and the x-direction variations in the displacement u are negligible along the segment 23. Equation (1) along segment 23 thus becomes:

$$J_h = \int_{23} T_y \cdot \frac{\partial v}{\partial x}\, dx = \Sigma\left[\left(\sigma_{yy} \cdot \frac{\Delta v}{\Delta x}\right)_i \Delta x_i\right]_{23} \tag{6}$$

where T_y is the surface traction in the y-direction.

Finally, the total J-integral value is given by:

$$J = 2(J_V + J_h) \tag{7}$$

To reiterate, while the approximate static J-integral in general will not yield the correct J-integral value associated with a propagating crack, the slow crack velocity of

$C/C_1 < 0.1$ and u small integration contour should increase the possibility of obtaining a reasonable estimate of the J-value.

EXPERIMENTAL PROCEDURE

Specimen

Figure 1 shows the Homalite-100 and 7075-T6 aluminum alloy SEN specimen used in this study. The abundant dynamic fracture data on Homalite-100 [1,12] provided a basis for assessing the accuracy of the proposed dynamic fracture analysis by moire interferometry. The initial crack of 25.4 mm in length was sharpened by chevron notching the tip with a razor blade. Crossed moire gratings of 600 lines/mm for the Homalite-100 SEN specimen were transferred to the specimens using the procedure developed by Post [15]. Crossed moire gratings of 150 lines/mm were used for 7075-T6 aluminum alloy SEN specimens.

Test Setup

The SEN specimens were loaded to failure in a hydraulic tensile testing machine. A two beam moire interferometry setup [15] was used to generate a reference grating of 1200 and 300 lines/mm for the Homalite-100 and 7075-T6 SEN specimens, respectively. These reference gratings interferred with the first order diffracted light from the specimen grating and effectively accomplished a 2X fringe multiplication of the specimen grating.

Four transient moire patterns were recorded by a specially configured IMACON 790 image converter camera. The image converter camera was triggered when the crack severed a line of conducting paint ahead of the crack tip. Unlike previous static analyses [9,10], the u- and v-displacement fields could not be recorded simultaneously due to the limited resolution of the camera. Thus a series of separate fracture tests, in which either the u- or the v-displacement field was recorded, were necessary to completely characterize the transient displacement field.

Data Reduction

As mentioned previously, only data from the near crack-tip field were used to determine the pertinent linear elasto-dynamic fracture parameters in this study. Thus an optimum orientation of a radial line, along which K_I^{dyn} and σ_{ox}^{dyn} could be determined accurately, was sought through a trial-and-error process. The moire fringe distributions in Figure 2 indicated that θ = 100° to 160° for the u-field and θ = 160° to 180° for the v-field appeared suitable for such purpose. At θ = 180° or along the crack surface, Equations (1) and (2) show that the u- and v-displacement fields will yield only σ_{ox}^{dyn} or K_I^{dyn}, respectively.

A sensitivity study using Equation (2) also shows that in the preferred region of θ = 100° to 180°, the v-displacement field is less sensitive to the variation in σ_{ox}^{dyn}. Thus the optimum θ values:

1) For K_I^{dyn} determination alone, θ = 180° using the v-field.

2) For K_I^{dyn} and σ_{ox}^{dyn} determination, θ = 120 to 150° using the u-displacement field.

The approximate J-integral values were evaluated along square contours with the crack tip in the center of the square using the static estimation procedure of Equation (6). The half-side length of the square contours varied from r = 3 to 10mm. The J-integral value is then equated to the strain energy release rate from which an approximate SIF can be derived. Error assessment of this static estimation procedure can be made by comparing the resultant SIF with K_I^{dyn} obtained by the COD procedure.

RESULTS

Figure 2 shows typical moire fringe patterns of the u- and v- displacements of two fracturing Homalite-100 SEN specimens. These moire fringes were used to determine K_I^{dyn} and σ_{ox}^{dyn} following the data reduction procedure described above. Specifically, the two adjacent moire fringe data at a radial distance of about r = 3 mm along a θ = const. radial line were used to evaluate K_I^{dyn} and σ_{ox}^{dyn} in this study.

Figure 3 shows plots of K_I^{dyn} versus crack velocity data obtained from the u- and v-displacement data. Also shown is the average K_I^{dyn} versus crack velocity relation, which was obtained nearly two decades ago [12], for the same batch of Homalite-100. Figure 4 shows the variations in σ_{ox}^{dyn}, which were obtained from the u-displacement data at four crack tip locations in three specimens.

The combined K_I^{dyn} and σ_{ox}^{dyn} were then substituted into the Equations (4) and (5) to check for possible crack curving and crack branching. The computed r_o for the data points in Figures 3 and 4 ranged from 10 mm to 40 mm which is much larger than the r_c = 1.3 mm obtained previously in [13]. Thus crack curving in these specimens was not a possibility. Needless to mention, crack branching, was precluded due to $K_I^{dyn} << K_{IB}$ where K_{IB} = 2.05 MPa$\sqrt{m}$ [14] and K_{IC} = 0.64 MPa$\sqrt{m}$ [12].

Figure 5 shows a typical transient Moire interferometry pattern corresponding to the u-displacement field in a fracturing 7075-T6 aluminum alloy SEN specimen. The moire fringe pattern for the v-displacement field, while sufficiently visible for data reduction, was blurred by the small but distinct wake of the crack tip plastic zone and is not presented here. Only two specimens were tested and thus the available data was not sufficient to construct a K_I^{dyn} versus crack velocity curve. Also, to the authors' knowledge, no dynamic characterization of thin 7075-T6 aluminum alloy sheets is available for comparison with the limited data obtained in this study. The tests (Figure 5) yielded K_I^{dyn} = 94 MPa$\sqrt{m}$ and σ_{ox}^{dyn} = 62 MPa$\sqrt{m}$. The former is about 1.6 times the K_{IC} = 58 MPa$\sqrt{m}$ and is consistent with the fact that the transient moire fringes were recorded immediately after the crack propagated from the somewhat blunt starter crack.

Figure 6 shows the variations in the normalized K_I obtained from an elastic analysis using the approximate J, which was calculated using Equation (7), with the size of the J-integral square contour for the Homalite-100 7075-T6 SEN specimens. The distance r in this figure represents one-half length of the side with the crack tip at the center of the square. The K_I, which was obtained through the J-integral, was normalized with the K_I^{dyn} which was obtained by the COD procedure. This figure shows that the static approximate

J-integral can be used to estimate the K_I^{dyn} if the contour is sufficiently small, i.e. r = 3 mm. Obviously this conclusion will differ for a crack running at a higher velocity and with the presence of a dominant biaxial stress field.

DISCUSSIONS

The K_I^{dyn} and σ_{ox}^{dyn} extraction procedure described in this paper is a straight forward use of the dynamic moire interferometry data. In practice, however, the caustics of the crack tip and trailing plastic zone in a somewhat ductile fracture specimen, such as 7075-T6 aluminum alloy, would obscure the moire fringes needed in deducing these fracture parameters using the COD procedure described here. For such cases, an "elastic analysis" using the approximate J-integral procedure may be more convenient to use as long as the integration contour can be made sufficiently small. When a power hardening stress-strain relation is used in place of the elastic analysis, the approximate J-integral will also provide a moderate plasticity correction provided the plasticity is limited to small scale yielding [9.10].

CONCLUSIONS

1. Dynamic moire interferometry can be used to determine the dynamic fracture parameters, such as K_I^{dyn} and σ_{ox}^{dyn}.

2. If u- and v-field displacements cannot be obtained simultaneously, then the u-displacement field is preferred for obtaining both K_I^{dyn} and σ_{ox}^{dyn} simultaneously. For K_I^{dyn} determination alone, the v-field displacement will suffice.

3. The static J-approximation procedure can be used to estimate K_I^{dyn} for a crack propagating at a moderate velocity.

ACKNOWLEDGEMENT

This research was supported by ONR contract N00014-89-J-1276. The authors are indebted to Dr. Yapa Rajapakse for his continued support and encouragement during the course of this investigation.

REFERENCES

1. J.W. Dally, "Dynamic Photoelastcity Studies of Fracture," Experimental Mechanics, Vol. 19, pp. 349-367, 1979.

2. W.B. Bradley and A.S. Kobayashi, "Fracture Dynamics - A Photoelastic Investigation," Engineering Fracture Mechanics, Vol. 3, pp. 317-332, 1971.

3. J.F. Kalthoff, J. Beinert and S. Winkler, "Measurements of Dynamic Stress Intensity Factors for Fast Running and Arresting Cracks in Double-Cantilever-Beam Specimens," Fast Fracture and Crack Arrest, ASTM STP 627, G.T. Hahn and M.F. Kanninen, pp. 161-176, 1977.

4. F. Katsamanis, D. Raftopulos and P.S. Theocaris, "Static and Dynamic Stress Intensity Factors by the Method of Transmitted Caustics," ASME Journal of Engineering Materials and Technology, Vol. 99, pp. 105-109, 1977.

5. K. Takahashi and K. Arakawa, "Dependence of Crack Acceleration on the Dynamic Stress-Intensity Factor in Polymers," Experimental Mechanics, Vol. 27, pp. 195-200, 1987.

6. A.S. Kobayashi, R.A. Selby and W.B. Bradley, "Transient Strains in a Fracturing Epoxy Plate With Central Notch," Proc. of the International Conference on Fracture, Vol. 3, eds, T. Yokobori, T. Kawasaki and J.L. Swedlow, Japan Society for Strength and Fracture of Metals, pp. 1809-1832, 1966.

7. A.S. Kobayashi, D.O. Harris and W.L. Engstrom, "Transient Analysis in a Fracturing Magnesium Plate," Experimental Mechanics, Vol. 7, No. 10, pp. 434-440, 1967.

8. D.B. Barker, R.J. Sanford and R. Chona, "Determining K and Related Stress-Field Parameters from Displacement Fields," Experimental Mechanics, Vol. 25, pp. 399-406, 1985.

9. M.S. Dadkhah and A.S. Kobayashi,"HRR Field of a Moving Crack, An Experimental Analysis," Engineering Fracture Mechanics, Vol. 34, No. 1, pp. 253-262, 1989.

10. M.S. Dadkhah, B.S.-J. Kang and A.S. Kobayashi, "J-Integral and HRR Field of a Stably Growing Crack, An Experimental Analysis," Proceedings of 9th International Conference on Experimental Mechanics, Vol. 5, Lyngby, Denmark, pp. 1767-1775, 1990.

11. Nishioka, T. and Atluri, S.N., "Path-Independent Integrals, Energy Release Rate, and General Solutions of Near-Tip Fields in Mixed-Mode Dynamic Fracture," Engineering Fracture Mechanics, 18, 1, pp. 1-22, 1983.

12. Kobayashi, A.S. and Mall, S., "Dynamic Fracture Toughness of Homalite-100," Experimental Mechanics, Vol. 18, No. 1, pp. 11-18, 1978.

13. Ramulu, M. and Kobayashi, A.S., "Dynamic Crack Curving-A Photoelastic Evaluation," Experimental Mechanics, Vol. 23, pp. 1-9, March 1983.

14. Ramulu, M. Kobayashi, A.S. and Kang, B.S.-J., "Dynamic Crack Branching-A Photoelastic Evaluation," Fracture Mechanics; Fifteenth Symposium, (ed.) R.J. Sanford, ASTM STP 833, pp. 130-148, 1984.

15. Kang, B.S. Kobayashi, A.S. and Post, D., "Stable Crack Growth in Aluminum Tensile Specimens," Experimental Mechanics, Vol. 27, pp. 234-245, 1987.

ASK/cm(1)

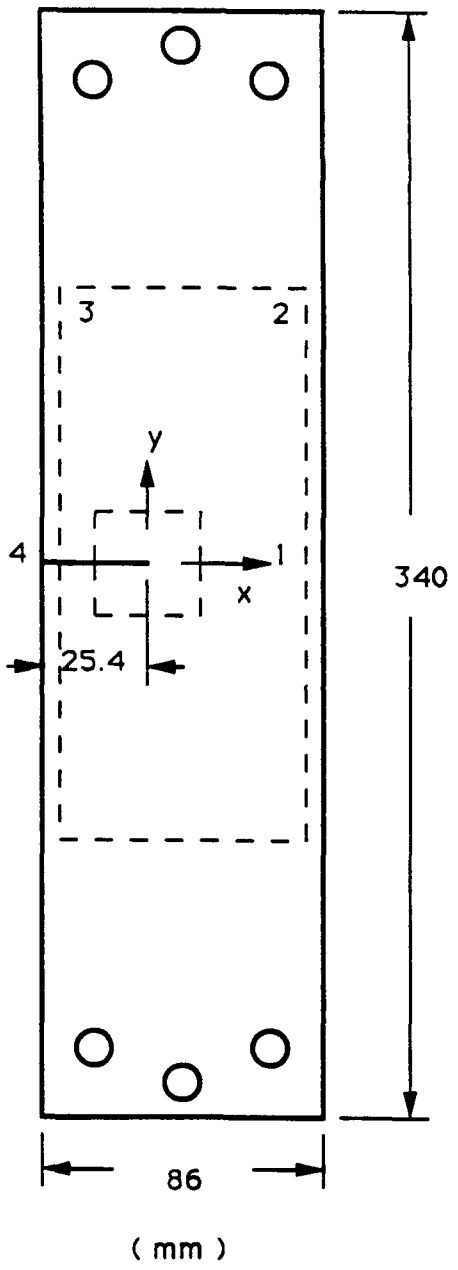

MATERIAL	THICKNESS (mm)
HOMOLITE-100	6
7075-T6	1

Figure 1. Specimen

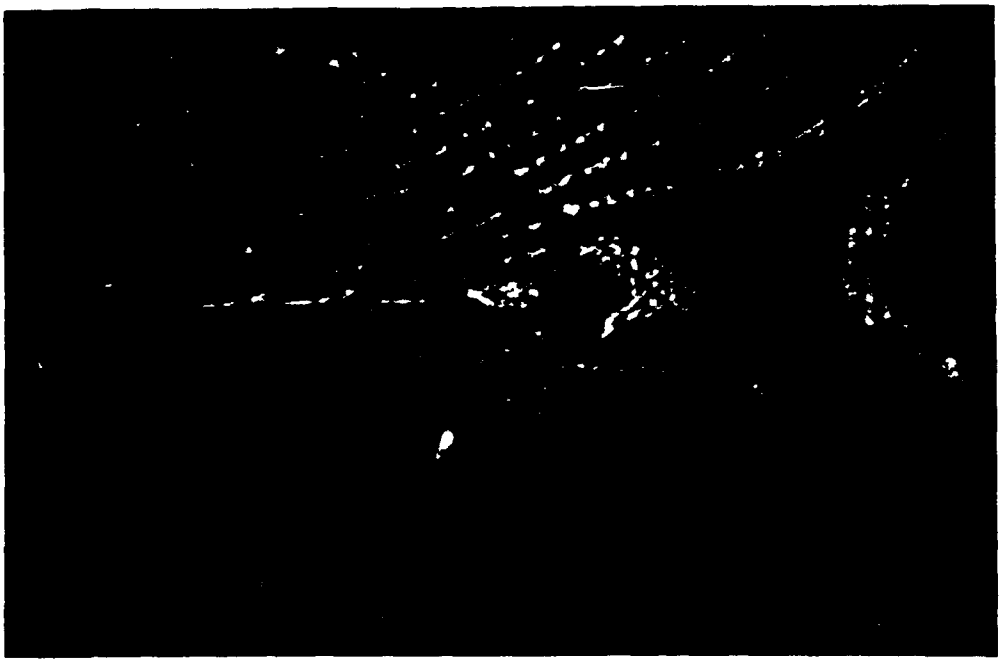

(a) u-displacement Field

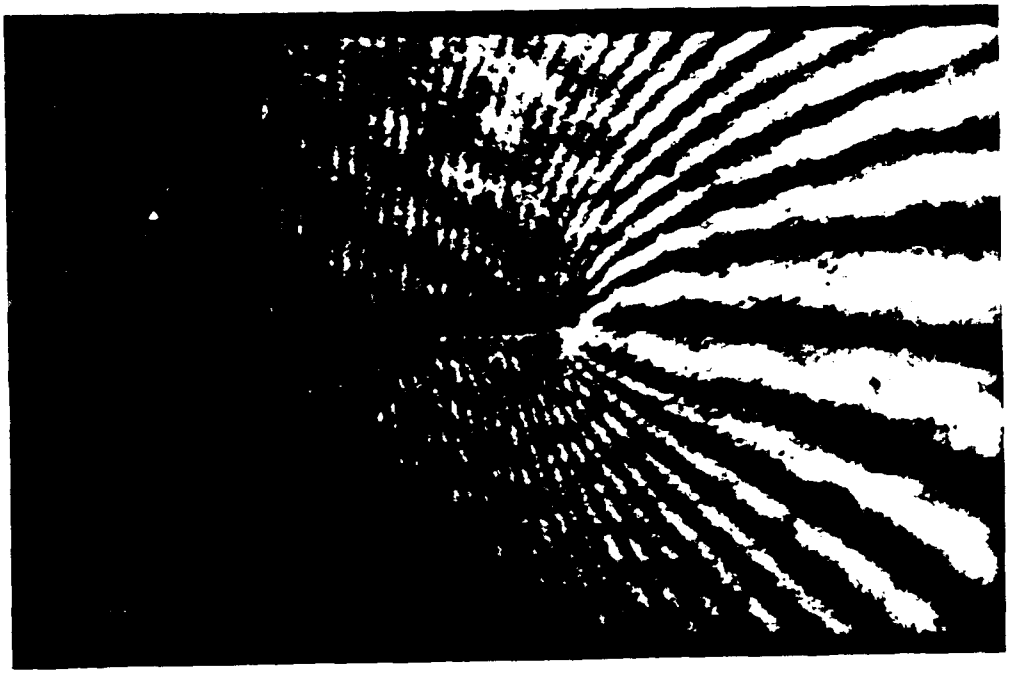

(b) v-displacement Field

Figure 2. Transient Moire Fringe Patterns in a Fracturing Homalite-100 Specimen.

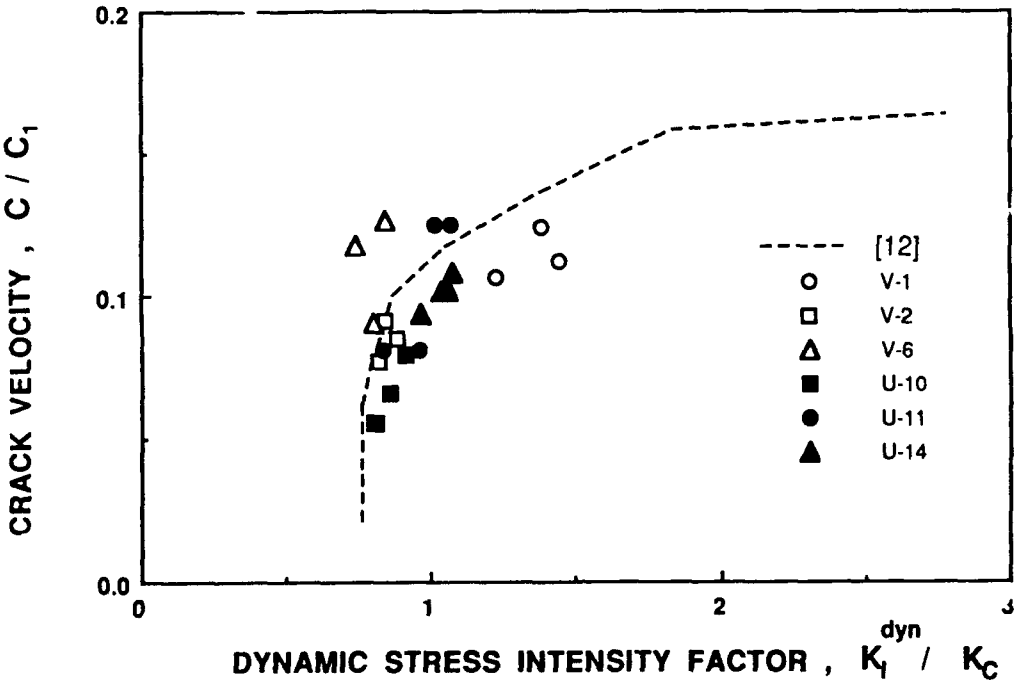

Figure 3. Dynamic Stress Intensity Factor versus Crack Velocity Relation of Homolite-100 Specimens.

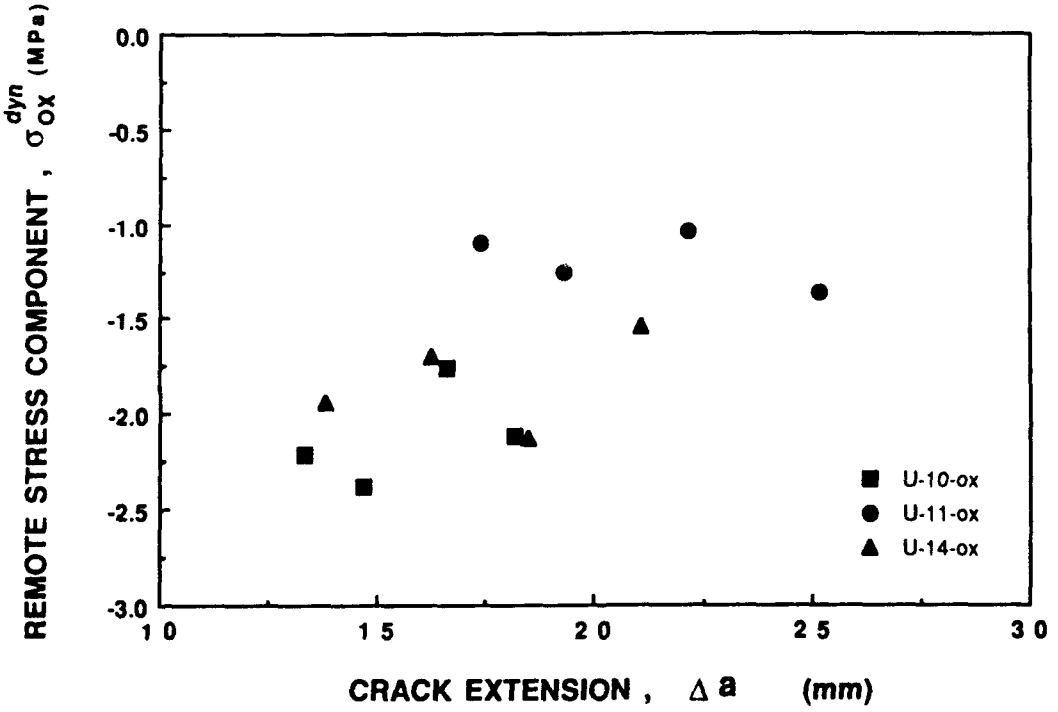

Figure 4. Variations in the Remote Stress Component with Crack Extension. Homalite-100 Specimens.

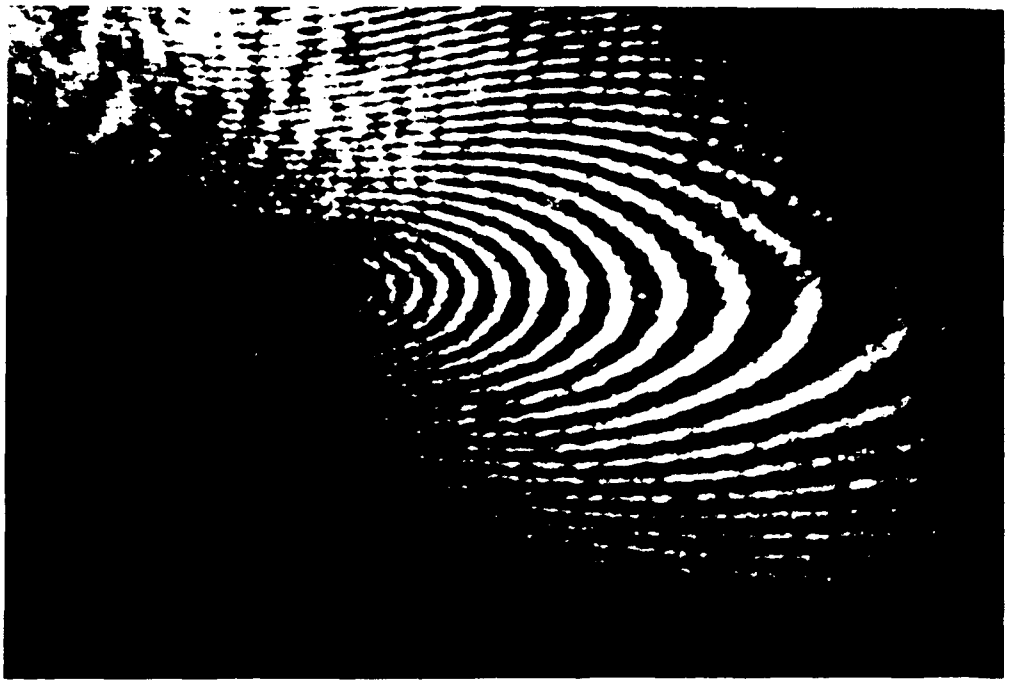

u-displacement Field

Figure 5. Transient Moire Fringe Pattern in a Fracturing 7075-T6 Specimen.

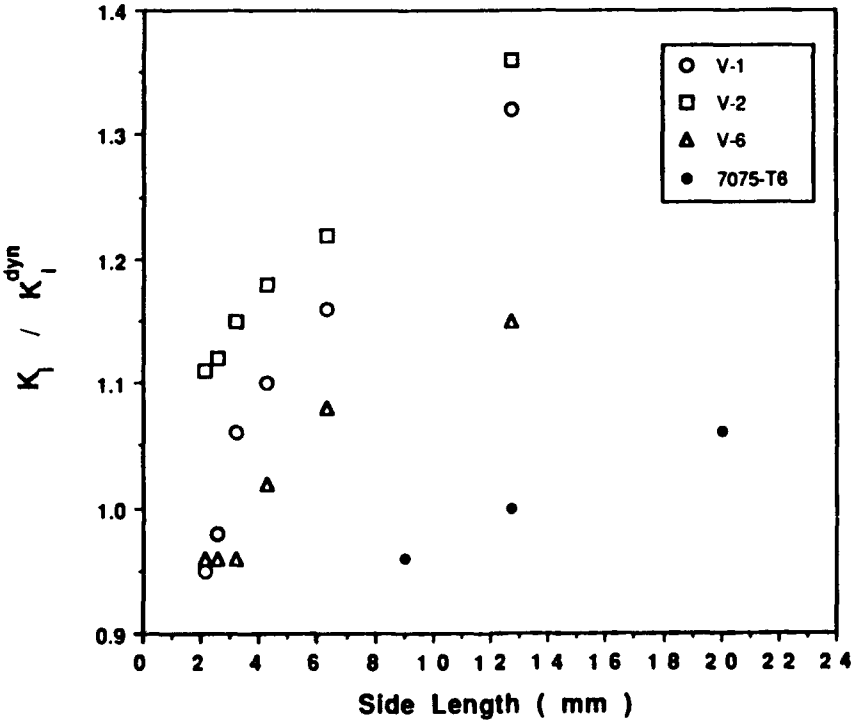

Figure 6. Normalized K_I^{dyn} Versus Half J-integral Contour Length.

Office of Naval Research
800 N Quincy Street
Arlington, VA 22217-5000
Attn: Code 11325M (4 copies)

Office of Naval Research
800 N Quincy Street
Arlington, VA 22217-5000
Attn: Code 1131

Defense Documentation Cntr
(4 copies)
Cameron Station
Alexandria, VA 02314

Naval Research Laboratory
Washington, DC 20375
Attn: Code 6000

Naval Research Laboratory
Washington, DC 20375
Attn: Code 6300

Naval Research Laboratory
Washington, DC 20375
Attn: Code 6380

Naval Research Laboratory
Washington, DC 20375
Attn: Code 5830

Naval Research Laboratory
Washington, DC 20375
Attn: Code 6390

Naval Research Laboratory
Washington, DC 20375
Attn: Code 2620

David W. Taylor Naval Ship
R & D Center
Annapolis, MD 21402
Attn: Code 28

David W. Taylor Naval Ship
R & D Center
Annapolis, MD 21402
Attn: Code 2812

David W. Taylor Naval Ship
R & D Center
Annapolis, MD 21402
Attn: Code 2814

David W. Taylor Naval Ship
R & D Center
Annapolis, MD 21402
Attn: Code 1700

David W. Taylor Naval Ship
R & D Center
Annapolis, MD 21402
Attn: Code 1720

David W. Taylor Naval Ship
R & D Center
Annapolis, MD 21402
Attn: Code 1720.4

Naval Air Development
Center
Warminster, PA 18974
Attn: Code 6043

Naval Air Development
Center
Warminster, PA 18974
Attn: Code 6063

Naval Surface Weapons
Center
White Oak, MD 20910
Attn: Code R30
Technical Library

Naval Surface Weapons
Center
Dahlgren, VA 22448
Attn: Technical Library

Naval Civil Eng Library
Port Hueneme, CA 93043
Attn: Technical Library

Naval Underwater Systems
Center
New London, CT 06320
Attn: Code 44
Technical Library

Naval Underwater Systems
Center
Newport, RI 02841
Attn: Technical Library

Naval Weapons Center
China Lake, CA 99555
Attn: Technical Library

NRL/Underwater Sound
Reference Dept.
Orlando, FL 32856
Attn: Technical Library

Chief of Naval Operations
Department of the Navy
Washington, DC 20350
Attn: Code OP-098

Commander
Naval Sea Systems Command
Washington, DC 20362
Attn: Code 05R25

Commander
Naval Sea Systems Command
Washington, DC 20362
Attn: Code 05R26

Commander
Naval Sea Systems Command
Washington, DC 20362
Attn: Code 09B31

Commander
Naval Sea Systems Command
Washington, DC 20362
Attn: Code 55Y

Commander
Naval Sea Systems Command
Washington, DC 20362
Attn: Code 55Y2

Commander
Naval Sea Systems Command
Washington, DC 20362
Attn: Code 03D

Commander
Naval Sea Systems Command
Washington, DC 20362
Attn: Code 7226

Commander
Naval Sea Systems Command
Washington, DC 20362
Attn: Code 310A

Commander
Naval Sea Systems Command
Washington, DC 20362
Attn: Code 310B

US Naval Academy
Mechanical Engineering Dept.
Annapolis, MD 21402

Naval Postgraduate School
Monterey, CA 93940
Attn: Technical Library

Mr. Jerome Persh
Stf Specit for Matls &Struct
OUSDE & E. The Pentagon
Room 301089
Washington, DC 20301

Professor J. Hutchinson
Harvard University
Div. of Applied Sciences
Cambridge, MA 02138

Dr. Harold Liebowitz, Dean
School of Engr. & Applied Sci.
George Washington
University
Washington, DC 20052

Professor G.T. Hahn
Penn State University
227 Hammond Bldg
University Park, PA 16802

Professor Albert S.
Kobayashi
Dept. of Mechanical
Engineering
University of Washington
Seattle, WA 98195

Professor L.B. Freund
Brown University
Division of Engineering
Providence, RI 02912

Professor B. Budiansky
Harvard University
Division of Applied Sciences
Cambridge, MA 02138

Professor S.N. Atluri
Georgia Institute of
Technology
School of Engr. & Mechanics
Atlanta, GA 30332

Professor G.Springer
Stanford University
Dept. of Aeronautics
& Astronautics
Stanford, CA 94305

Professor H.T. Hahn
Dept of Engr Sciences &
Mech
Penn State University
227 Hammond Bldg
University Park, PA 16802

Professor S.K. Datta
University of Colorado
Dept. of Mechanical
Engineering
Boulder, CO 80309

Dr. M.L. Williams
School of Engineering
University of Pittsburgh
Pittsburgh, PA 15261

Professor R.H. Gallagher
President
Clarkson University
Potsdam, NY 13676

Dr. D.C. Drucker
Dept. of Aerospace Eng.
& Mechanics
University of Florida
Tallahassee, FL 32611

Professor B.A. Boley
Columbia University
Dept. of Civil Engineering &
Engineering Mechanics
New York, NY 10027

Professor J. Dulfy
Brown University
Division of Engineering
Providence, RI 02912

Professor J.D. Achenbach
Northwestern University
Dept of Civil Engineering
Evanston, IL 60208

Professor F.A. McClintock
Dept of Mechanical
Engineering
Massachusetts Institute of
Technology
Cambridge, MA 02139

Professor D.M. Parks
Dept of Mechanical
Engineering
Massachusetts Institute of
Technology
Cambridge, MA 02139

Dr. M.F. Kanninen
Southwest Research
Institute
PO Drawer 28510
6220 Culebra Road
San Antonio, TX 78284

Professor F.P. Chiang
Dept of Mechanical Engr
State U of NY at Stony Brook
Stony Brook, NY 11794

Professor S.S. Wang
Dept of Theoretical & Appl
Mechs
University of Illinois
Urbana, IL 61801

Professor Y. Weitsman
Civil Engr Department
Texas A&M University
College Station, TX 77843

Professor I.M. Daniel
Dept of Mechanical Engr
Northwestern University
Evanston, IL 60208

Professor C.T. Sun
School of Aeronautics
& Astronautics
Purdue University
W. Lafayette, IN 47907

Professor J. Awerbuch
Dept of Mech Engr &
Mechanics
Drexel University
Philadelphia, PA 19104

Professor T.H. Lin
University of California
Civil Engineering Dept
Los Angeles, CA 90024

Professor G.J. Dvorak
Dept of Civil Engr
Rensselaer Polytecnic
Institute
Troy, NY 12180

Dr. R.M. Christensen
Chemistry & Mtrl Sci Dept
Lawrence Livermore Natl L
PO Box 80P
Livermore, CA 94550

Professor J.R. Rice
Division of Applied Scienc
Harvard University
Cambridge, MA 02138

Professor W.N. Sharpe
The Johns Hopkins
University
Dept of Mechanics
Baltimore, MD 21218

Professor C.F. Shih
Brown University
Division of Engineering
Providence, RI 02912

Professor A. Rosakis
California Institute of Tecl
Graduate Aeronautical Lat
Pasadena, CA 91125

Professor D. Post
VA Polytechnic & State U
Dept of Engr Science &
Mechanics
Blacksburg, VA 24061

Professor W. Sachse
Cornell University
Dept of Theoretical &
Applied Mechanics
Ithaca, NY 14853

Unclassified

SECURITY CLASSIFICATION OF THIS PAGE (When Data Entered)

REPORT DOCUMENTATION PAGE		READ INSTRUCTIONS BEFORE COMPLETING FORM
1. REPORT NUMBER UWA/DME/TR-90/ 68	2. GOVT ACCESSION NO.	3. RECIPIENT'S CATALOG NUMBER
4. TITLE (and Subtitle) Dynamic Fracture Analysis by Moire Interferometry		5. TYPE OF REPORT & PERIOD COVERED Technical Report 6. PERFORMING ORG. REPORT NUMBER UWA/DME/TR-90/68
7. AUTHOR(s) K. Arakawa, R.H. Drinnon, M. Kosai and A.S. Kobayashi		8. CONTRACT OR GRANT NUMBER(s) N00014-89-J-1276
9. PERFORMING ORGANIZATION NAME AND ADDRESS Department of Mechanical Engineering, FU-10 University of Washington Seattle, Washington 98195		10. PROGRAM ELEMENT, PROJECT, TASK AREA & WORK UNIT NUMBERS
11. CONTROLLING OFFICE NAME AND ADDRESS Office of Naval Research Arlington, Virginia 22217		12. REPORT DATE 1990 13. NUMBER OF PAGES 12
14. MONITORING AGENCY NAME & ADDRESS(if different from Controlling Office)		15. SECURITY CLASS. (of this report) Unclassified 15a. DECLASSIFICATION/DOWNGRADING SCHEDULE

16. DISTRIBUTION STATEMENT (of this Report)

Unlimited

17. DISTRIBUTION STATEMENT (of the abstract entered in Block 20, if different from Report)

18. SUPPLEMENTARY NOTES

19. KEY WORDS (Continue on reverse side if necessary and identify by block number)

Moire Interferometry, Dynamic Fracture Mechanics, Dynamic Stress Intensity Factor.

20. ABSTRACT (Continue on reverse side if necessary and identify by block number)

Dynamic moire interferometry was used to measure separately the u- and v-displacement fields surrounding a rapidly propagating crack tip. Four transient moire patterns with an effective line density of 1200 lines/mm were recorded for each fracturing specimen by a specially configured IMACON 790 image converter camera. The dynamic crack tip displacement field by Nishioka et al was then used to determine the dynamic stress intensity factor and remote stress component from the transient crack tip displacement data of fracturing Homalite-100 and 7075-T6 aluminum alloy plates.

DD FORM 1 JAN 73 1473 EDITION OF 1 NOV 65 IS OBSOLETE
S/N 0102-014-6601

Unclassified
SECURITY CLASSIFICATION OF THIS PAGE (When Data Entered)